NANO LETTERS

Letter

pubs.acs.org/NanoLett

Efficient Photon Capturing with Ordered Three-Dimensional Nanowell Arrays

Siu-Fung Leung,[†,§] Miao Yu,[†,§] Qingfeng Lin,[†,§] Kyungmook Kwon,[‡] Kwong-Lung Ching,[†] Leilei Gu,[†] Kyoungsik Yu,[‡] and Zhiyong Fan*[,†]

[†]Department of Electronic and Computer Engineering, Hong Kong University of Science and Technology, Clear Water Bay, Kowloon, Hong Kong, China SAR

[‡]Department of Electrical Engineering, Korea Advanced Institute of Science and Technology, Daejeon 305-701, Korea

Supporting Information

ABSTRACT: Unique light-matter interaction at nanophotonic regime can be harnessed for designing efficient photonic and optoelectronic devices such as solar cells, lasers, and photodetectors. In this work, periodic photon nanowells are fabricated with a low-cost and scalable approach, followed by systematic investigations of their photon capturing properties combining experiments and simulations. Intriguingly, it is found that a proper periodicity greatly facilitates photon capturing process in the nanowells, primarily owing to optical diffraction. Meanwhile, the nanoengineered morphology renders the nanostructures with a broad-band efficient light absorption. The findings in this work can be utilized to implement a new type of nanostructure-based solar cells. Also, the methodology applied in this work can be generalized to rational design of other types of efficient photon-harvesting devices.

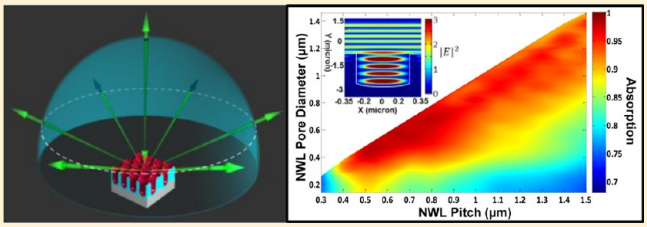

KEYWORDS: *Nanophotonics, nanowell array, photon capturing, optical diffraction grating, photovoltaics*

Efficient photon harvesting is crucial for many types of optoelectronic devices such as photodetectors and solar cells. Three-dimensional (3D) nanostructures made of photonic materials have demonstrated highly promising capability of harvesting incoming photons from a wide angle with a broad wavelength range.[1−4] Specifically, arrays of a variety of 3D nanostructures, such as nanopyramids,[5,6] nanowires,[1,7−11] nanopillars,[12,13] nanocones,[1,14,15] spherical nanostructures,[16,17] and so forth, have been extensively and successfully fabricated for light trapping and solar energy conversion with materials including Si,[1,7,9] Ge,[3,12] CdS,[13] CIGS,[2] and ZnO.[11] In fact, most of these nanostructures can be categorized as "positive" structures with respect to substrates, namely, structures are protruding out from substrates to free space. In contrast, there are only very few reports on photon trapping in deep "negative" nanostructures, for example, nanoholes (NHLs), and nanowells (NWLs).[18,19] Mainly due to the limited choice on fabricating these nanostructures with well-defined and tunable pitch, pore diameter, and depth, as compared to the vast choice of fabrication methods for "positive" 3D nanostructures, including etching,[1,7] chemical vapor deposition,[3,9,13] electrodeposition,[20,21] and so forth. In general, light trapping in the "positive" nanostructure arrays can be simply described as the result of photon multiple scattering within the nanostructures, which increases effective optical path length of a photon and absorption probability.[5,22] Nevertheless, structures such as NHLs and NWLs with cylindrical cavities provide geometric confinement for incoming photons naturally, thus photon trapping process is expected to be different. In fact, theoretical simulations have revealed that NHL arrays can outperform nanorod arrays for practical thickness of light absorbing material.[19] In addition, properly designed NHLs and NWLs can be also used as templates for thin film devices, for example, solar cells, as in the case of improving solar cell performance with "positive" 3D nanostructures.[23,24] Therefore, understanding light trapping in engineered NHLs and NWLs is not only of fundamental interest, but also of technological importance. In this regard, we have fabricated perfectly ordered flexible 3D arrays of NWLs with largely tunable well pitch, diameter, and depth based on a self-organized approach without using optical lithographic method explored previously.[18] In order to understand photon-trapping processes in regular NWL arrays, thin films of light absorbing material were conformally coated in the NWLs followed by systematic experimental and theoretical investigations of their optical absorption properties. It was found that light-trapping behavior of NWLs varies significantly while tuning their diameter and pitch independently. Also, the periodicity of NWLs plays a crucial role in photon capturing process. Specifically, strong diffraction of light greatly enhances photon capturing capability leading to absorption band observed on the geometric 2D absorption contour. Interestingly, it was revealed that a

Received: April 18, 2012
Revised: May 19, 2012
Published: May 28, 2012

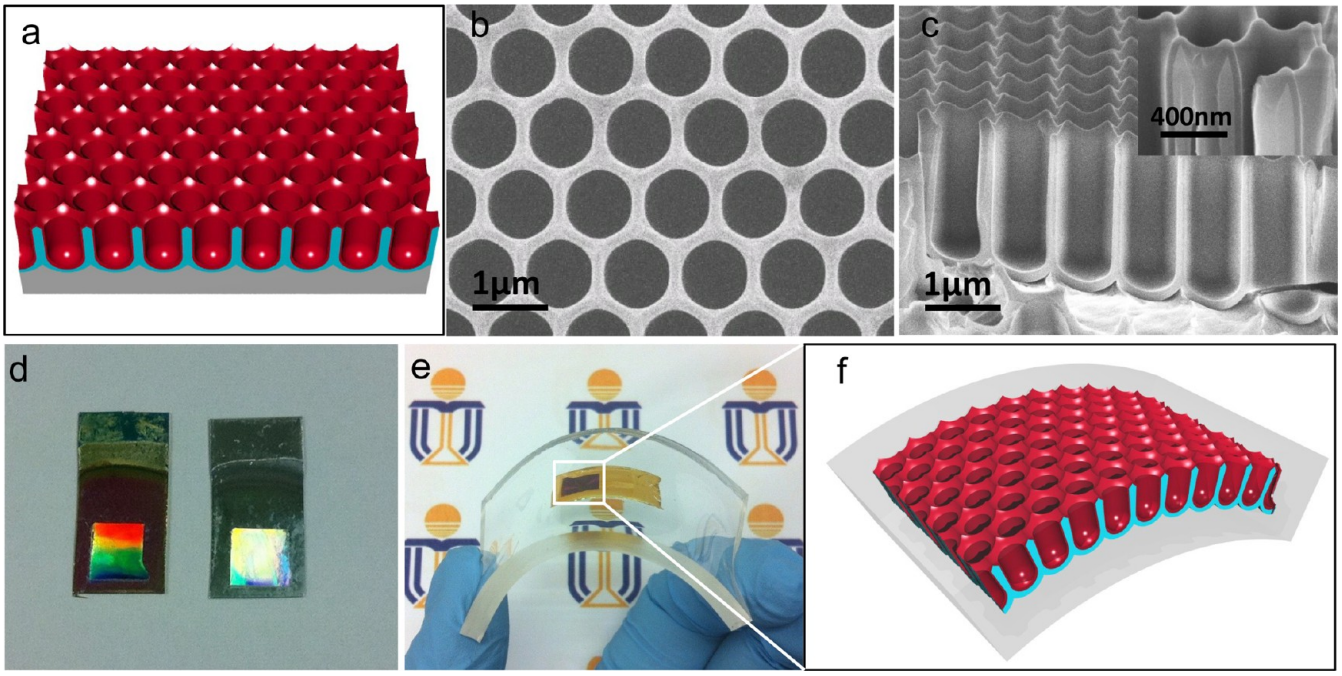

Figure 1. (a) Schematic drawing of ordered NWLs fabricated on Al substrate with red color representing conformal a-Si coating. (b) Top view SEM image of the 1 μm pitch NWL sample with NWL diameter widened to 870 nm by wet etching. (c) Cross-section of a 1 μm pitch NWL sample with 50 nm a-Si conformal coating. Inset: high-magnification SEM image showing uniform a-Si coating on NWL side wall. (d) Photograph of NWL samples with a-Si (left photo) and without a-Si (right photo) coating. (e,f) Photo and schematic of flexible NWLs embedded in polydimethylsiloxane (PDMS).

matching condition between optical wavelength and the periodicity results in efficient photon coupling into NWLs with subwavelength diameter and subsequent absorption.

The ordered NWL arrays in this work were fabricated using nanoimprint process in conjunction with stable high voltage anodization of aluminum (Al) foil. The detailed fabrication process for hexagonally ordered NWLs can be found in the Supporting Information Figure S1. It is well-known that Al anodization forms self-organized nanoporous alumina structures.[25] These nanostructures have been widely utilized for direct assembly of nanomaterials as nanoengineering templates.[12,13,26−28] However, conventionally Al anodization can yield ordered alumina nanopores with pitch and diameter up to 500 nm,[29,30] which limits the light-structure interaction for long wavelengths in the solar spectrum. In this work, we have developed a greatly improved Al anodization technique to fabricate alumina NWLs with perfect hexagonal ordering extending to centimeter scale with a wide range of NWL pitches and diameters from ~400 nm up to 1.5 μm (Supporting Information Figure S2). Figure 1a demonstrates a schematic of the fabricated NWLs on Al supporting substrate with the red color layer representing a conformal coating of 50 nm a-Si film serving as light absorber. In addition, the top surface of NWL array has periodic roughness coming from the two-step anodization (Supporting Information Figure S1). This unique feature leads to additional photon scattering mechanism that will be further discussed later. Figure 1b,c demonstrates top view and cross-sectional view scanning electron microscopy (SEM) images of a 1 μm pitch NWL sample, showing uniform NWL diameter of 870 nm with conformal a-Si coating with low pressure chemical vapor deposition (LPCVD).

It is worth pointing out that the NWLs fabricated here have hemispherical bottom with Al supporting substrate serving as the backside reflector, therefore, the NWLs are in fact one-end-open cavities for photon trapping. Figure 1d shows a photograph of two 1 μm pitch samples with (left sample) and without (right sample) 50 nm a-Si conformal coating. As the NWL arrays have perfect hexagonal ordering, both of the samples show diffraction of room light, however, the sample with 50 nm a-Si film demonstrates much lower diffraction intensity indicating photon trapping effect. In addition, as the thickness of the NWL arrays is only 2 μm, they can be readily detached from Al substrate and embedded in flexible substrate, as shown in Figure 1e,f, following the previously developed approach.[12] This unique property is highly attractive for flexible photonic and optoelectronic applications.

In order to investigate the effect of the geometry of the NWLs on their light trapping property, NWLs with seven different pitches from 364 nm to 1.5 μm were fabricated. And for each pitch, NWLs with 5−7 different diameters were also obtained. The details of their geometry can be found in Supporting Information Table S2. To understand their optical properties, UV−vis reflective spectra were obtained with an integrating sphere. Because the samples are opaque, their absorption spectra were obtained by subtracting reflectance from unity. Figure 2a demonstrates the absorption spectra of 500 nm pitch NWLs with 2 μm depth and five different diameters ranging from 161 to 442 nm. It is known that optical band gap of a-Si is ~1.7 eV, corresponding to ~720 nm optical wavelength. Therefore, spectral range 300−720 nm was chosen to investigate above-band gap optical absorption of NWLs. On the other hand, this wavelength range has covered the peak of solar irradiance, as shown in the inset of Figure 2a, thus the results are meaningful for further photovoltaic studies. As it can be clearly observed in Figure 2a, 500 nm pitch NWL arrays yield humps of absorption centering around 500 nm wavelength. Large NWL pore size favors light trapping apparently, especially for long wavelength. Particularly, the NWL array with

dx.doi.org/10.1021/nl3014567 | Nano Lett. 2012, 12, 3682−3689

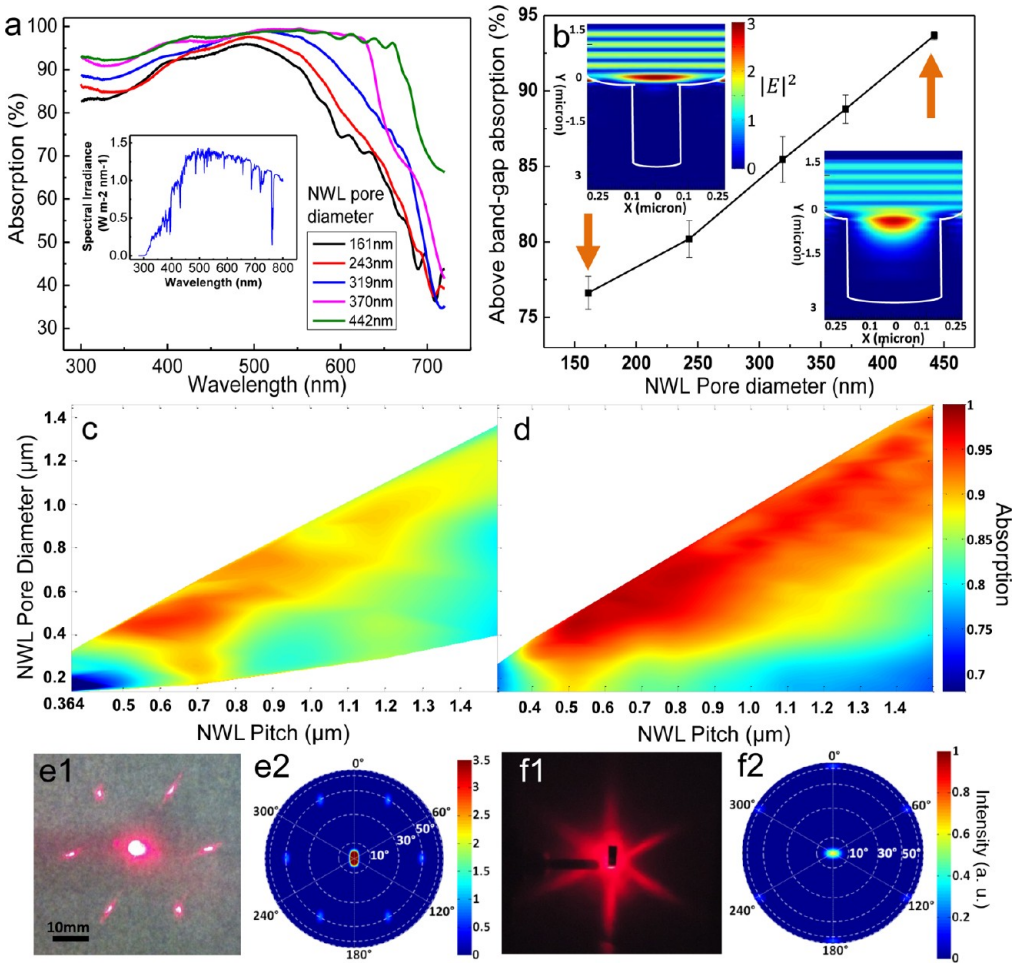

Figure 2. (a) Optical absorption spectra of 500 nm pitch NWLs with diameters from 161 to 442 nm with 50 nm thick a-Si conformal coating. Inset: spectral irradiance of AM 1.5 solar spectrum with 300−720 nm wavelength range. (b) Solar spectrum weighted above-band gap absorption of 500 nm pitch NWLs with varying pore diameter. Insets: simulated $|E|^2$ cross-sectional distribution inside NWLs with diameter of 150 nm (left inset) and 450 nm (right inset). (c) The experimental and (d) the simulated 2D contours of above-band gap absorption plotted as a function of NWL pore diameter and pitch. (e1,f1) Diffraction patterns of 1 μm and 700 nm NWL array samples generated with 650 nm diode laser. (e2,f2) Simulated diffraction patterns for 1 μm and 700 nm NWL array samples using 650 nm wavelength plotted in hemispherical coordinate system.

442 nm pore diameter has demonstrated 99.2% absorption at 550 nm wavelength. In order to evaluate the broadband absorption capability of NWL arrays, their absorption spectra were integrated with the solar spectrum (AM 1.5) shown in the inset of Figure 2a, resulting in above-band gap broadband absorption shown in Figure 2b. Evidently, above-band gap absorption monotonically increases with NWL pore diameter, approaching 94% for 442 nm NWL diameter. In order to understand this trend, finite difference time domain (FDTD) simulations (Lumerical 7.5, Supporting Information) were performed on the NWL arrays with pore diameter 160 and 450 nm at 650 nm wavelength, and the cross-sectional electric field intensity ($|E|^2$) distribution of the electromagnetic (EM) wave was plotted as the insets of Figure 2b. In these two simulations, EM plane waves propagate downward from Y = 1.5 μm and reach the top surfaces of nanostructures at Y = 0 μm. Thereafter, part of the EM waves is reflected by the top surfaces, forming interference fringes with the incoming waves. The rest part of energy of EM waves is either absorbed by a-Si thin film on top surfaces or coupled into NWLs subject to further absorption process. Note that the color index at the specific location in the simulations reflects the magnitude of $|E|^2$ at that point, normalized with that of the source EM wave if propagating in free space. It can be observed that the 450 nm diameter NWL array sample demonstrates quite low reflectance (right inset), indicated by the fact that the interference fringes are obscure and the highest color index of the interference fringes is close to unity. Meanwhile, propagation of EM wave into NWL in this case is visible, demonstrating a quick decay of intensity down to 1 μm depth due to significant absorption. On the other hand, simulation of 160 nm diameter NWL array sample (left inset) clearly shows much stronger reflectance from the top surface of the structure that is attributed to a combinational effect of inefficient photon coupling into deep subwavelength NWL and large top structure surface area.

To further understand photon trapping in NWL arrays with different geometries, above-band gap broadband absorption for NWL arrays with pitches from 364 nm to 1.5 μm and different NWL diameters was obtained and plotted as a semi-2D contour with pitch as X-axis, NWL diameter excluding 50 nm a-Si as Y-axis and color representing the solar spectrum weighted absorption, shown in Figure 2c. In order to achieve a credible 2D contour, enough number of different NWL geometries has been obtained, as shown in Supporting Information Table S2. Eventually this 2D contour was acquired by using absorption data of these actual structures and linear data interpolation.

dx.doi.org/10.1021/nl3014567 | Nano Lett. 2012, 12, 3682−3689

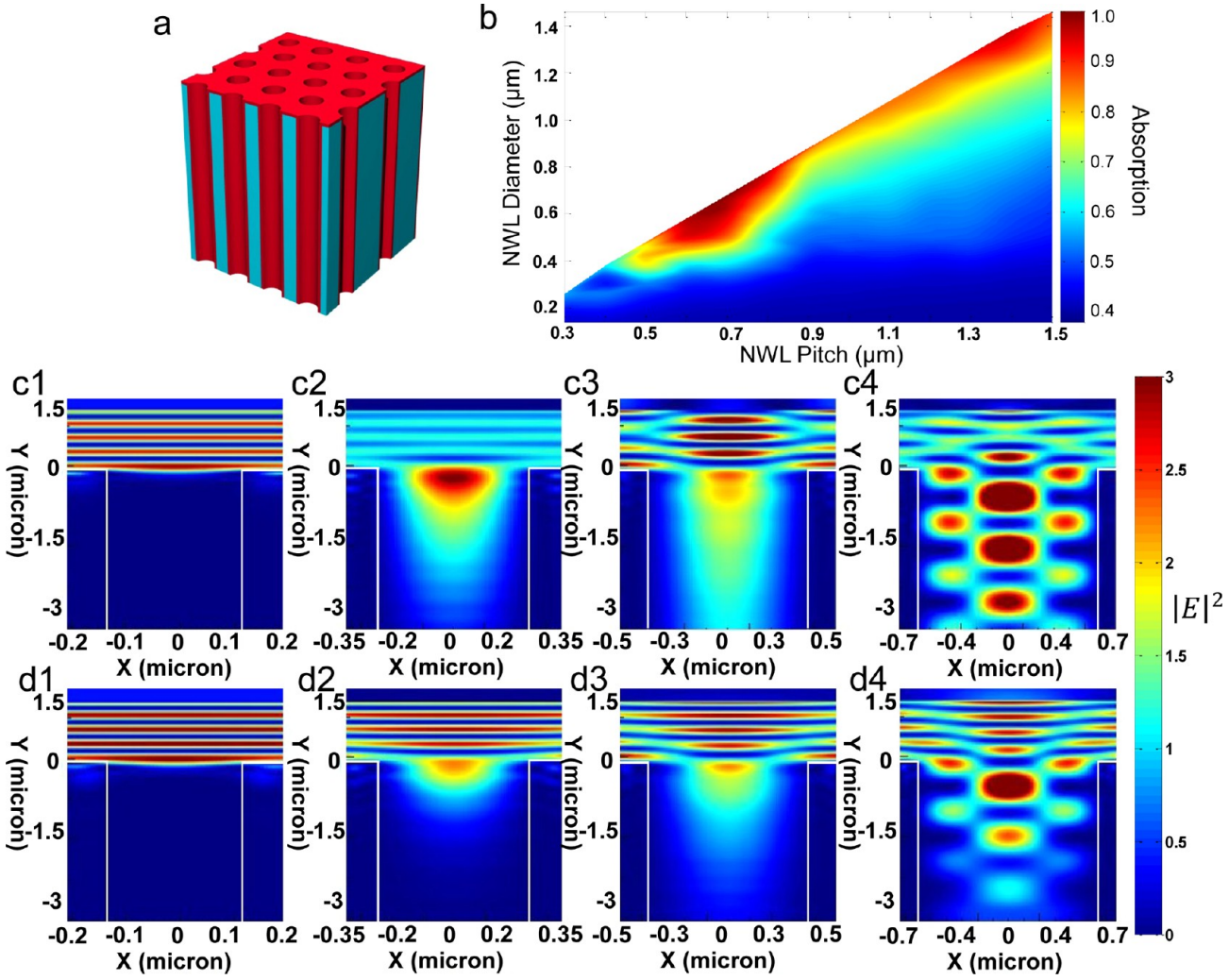

Figure 3. (a) Schematic drawing of ordered semi-infinitive deep NWLs. (b) Simulated absorption 2D contour with a monochromatic input light λ = 700 nm showing two absorption bands centering around pitch $d = \lambda$ and 2λ. (c1−c4) Simulated $|E|^2$ cross-sectional distribution inside NWLs with pitches of 400 nm, 700 nm, 1 μm, and 1.4 μm, respectively, showing efficient photon capturing when pitch $d = \lambda$ and 2λ. In these cases, NWL pore sizes are 100 nm smaller than the pitches. (d1−d4) $|E|^2$ cross-sectional distribution inside NWLs with the same pore diameter corresponding to (c1−c4), however, these NWLs are isolated structures without periodicity.

Note that in this 2D contour, the diagonal boundary indicates the maximum NWL pore size for the corresponding pitch fabricated experimentally for each pitch, and the lower boundary above *X*-axis shows the as grown NWL pore size in experiments without wet etching. From Figure 2c, it can be clearly observed that there is an absorption band extending from 500 to 900 nm pitch, along the diagonal boundary of the 2D contour with the highest absorption of 94.4%. This observation is also consistent with the simulated 2D contour with FDTD in which pitch and pore size were tuned with smaller step than experiments, as shown in Figure 2d. Note that the simulated nanostructures have the periodic top roughness, as shown in Figure 1a,c, in order to closely match experiments. Both the experimental and the simulated 2D contours show high absorption with only 2 μm depth of NWLs on Al substrates. In fact, it was found that the absorption was marginally reduced after removing Al backside reflector (Supporting Information Figure S3), especially for NWL arrays with pitch less than 1 μm, which indicates strong light absorption capability of NWL arrays.

The fact that both experimental and simulation results show an absorption band centering around 700 nm pitch and large pore size is intriguing. It coincides with the peak location of photon flux of AM 1.5 spectrum as shown in Supporting Information Figure S4, which suggests that a matching condition between the pitch of NWL arrays and wavelength of the majority photons leads to efficient photon capturing. In order to interpret this phenomenon, further experiments and simulations were performed. First, a diode laser with wavelength 650 nm, which is the closest one to 700 nm that we have obtained, was used as a monochromatic light source to observe the diffraction from NWL arrays with different pitches at the largest pore sizes. The measurement configuration is schematically shown in Supporting Information Figure S5. In brief, the laser beam was shined normally onto an NWL array through a 3 mm hole on a semitransparent paper screen. Then the diffracted beams were projected onto the backside of the paper screen indicating their locations. As the NWL arrays have perfect hexagonal ordering, first order diffraction patterns of light can be clearly resolved on the screen from the laser side for the 1 μm pitch NWL array, shown in Figure 2e1, with the

dx.doi.org/10.1021/nl3014567 | *Nano Lett.* 2012, 12, 3682−3689

zeroth order returning back through the hole. In fact, the angle of the first order diffraction from normal can be readily measured to be 43°. Meanwhile, it was also consistently calculated to be 41°, following simple diffraction grating equation $d \sin \theta = m\lambda$,[31] where d is the grating lattice constant, that is, NWL pitch in this work, θ is the diffraction angle, m is the diffraction order, and λ is the wavelength. Apparently, for d = 1 μm and λ = 650 nm, $m \leq 1$. Furthermore, the diffraction pattern has also been simulated with FDTD and observed from far field in a hemispherical coordinate system (Supporting Information Figure S5b), as shown in Figure 2e2, yielding θ = 47°.

In general, diffraction of light can be understood as the reflected light gaining horizontal momentum from the periodic grating structure according to the well-developed grating theory.[31] This can increase the optical path length of photons in the 3D NWL array structure leading to increased absorption probability. Naturally, this improvement largely depends on the diffraction angle, that is, the larger the diffraction angle, the longer the photons travel path in the structure and the better they are confined in NWLs. Ideally, when $m\lambda$ is approaching d from the shorter wavelength, θ is approaching 90° from the smaller angle thus the mth diffracted light will be propagating in plane inside the NWL array structures, maximizing the photon absorption probability. In our experiments, the closest match between laser wavelength and NWL array pitch is 650 nm laser with 700 nm pitch and the first order diffraction angle can be calculated as 68°. Figure 2f1 shows the picture of the corresponding diffraction pattern. Because of the significantly lower diffraction intensity and larger angle of the first order diffraction as compared to that of 1 μm pitch sample (Figure 2e1), the diffraction pattern cannot be clearly seen thus the picture was taken from the sample side (Supporting Information Figure S5a) in completely dark environment, indicating strong light absorption by the NWL array. Figure 2f2 demonstrates the far-field simulated diffraction pattern, showing consistently 73° angle for the first order diffraction, and much weaker intensity of both the zeroth and first order diffraction as compared to Figure 2e2.

For a 2D diffraction grating, a matching condition between incident wavelength and grating constant ($d = m\lambda$) results in the mth order diffraction grazing the surface of the grating, causing extraordinary low reflectance previously defined as Wood Anomaly.[31] In fact, our experiments have shown that strong light absorption can be achieved even there is a small mismatch, for example, 650 nm incident light and 700 nm pitch. This can be rationalized as the result of 3D NWL geometry, in this case even 68° diffraction angle is enough to cause significant absorption. This characteristic is particularly useful for efficient light trapping if the incident light is broadband. In addition, the above rationale can be also used to interpret spectral absorption for d = 500 nm with different NWL diameter, shown in Figure 2a, demonstrating the best absorption occurs around 500 nm wavelength for all diameters. On the other hand, since diffraction order m can be higher than 0 and 1, depending on the relationship between pitch d and wavelength λ, diffraction patterns of pitches of 700 nm, 1.2 μm, and 1.5 μm were also recorded and shown in Supporting Information Figure S6 in which the 1.5 μm pitch sample demonstrates both first and second order diffraction. The measured, calculated, and simulated diffraction angles are consistently shown in Supporting Information Table S3. Note that both transverse electric field (TE) and transverse magnetic field (TM) modes were used for simulations, and there is no significant difference observed as shown in Supporting Information Figure S6.

According to the grating equation $d \sin \theta = m\lambda$, one may expect that when the second order diffraction is approaching to 90°, that is, $d = 2\lambda$, there should be another absorption band on the geometric 2D absorption contour. However, it is not obvious in Figure 2c,d, around d = 1.2−1.4 μm. To shed more light on this contradiction, further simulations were performed. As the current NWLs have only 2 μm depth with a-Si bottoms and reflective Al supporting substrate at the bottom, optical reflectance can come from both the top and bottom of NWLs. In order to simplify the situation to gain more fundamental insight of optical property of NWL structures, NWLs with "semi-infinitive" depth and without top surface roughness, as shown in Figure 3a, were simulated with normal incident single wavelength λ = 700 nm. Figure 3b demonstrates a 2D absorption contour of the corresponding structure, indicating the capturing efficiency of 700 nm wavelength photons into the structure. It is evident that there are indeed two efficient bands for photon capturing, centering around 700 nm (λ) and 1.4 μm (2λ) pitches with large NWL diameters. In fact, simulations with 400, 500, and 600 nm wavelengths consistently demonstrate absorption bands at $n\lambda$ (n = 1, 2, 3) locations on the 2D contours shown in Supporting Information Figure S7.

In order to understand EM wave coupling and propagation in the semi-infinitive NWLs with 700 nm wavelength, distribution of $|E|^2$ at the cross sections of NWLs with pitches of 400 nm, 700 nm, 1 μm, and 1.4 μm and diameters 100 nm less than the pitches are shown in Figure 3c1, c2, c3 and c4, respectively. Akin to the insets in Figure 2b, the color index of the interference fringes in Figure 3c between Y = 1.5 μm and Y = 0 μm indicates the intensity of the reflected EM wave. It can be clearly seen that 400 nm pitch condition (Figure 3c1) yields very low photon capturing efficiency; the majority energy of EM wave is reflected and almost no energy is coupled into NWL. This observation can be attributed to the fact that NWL diameter is only 300 nm, which is much smaller than wavelength (λ = 700 nm). However, 700 nm pitch condition yields distinctive difference, as shown in Figure 3c2, reflectance is much weaker, and the significant part of EM wave energy is coupled into NWL although the NWL diameter is 100 nm smaller than the wavelength. Furthermore, 1 μm pitch NWL (Figure 3c3) shows stronger reflectance than 700 nm pitch though the NWL diameter is much larger, and 1.4 μm pitch NWL (Figure 3c4) demonstrates low reflectance and clearly much better photon coupling in NWL than 1 μm pitch condition again. These results are consistent with the 2D absorption contour shown in Figure 3b, indicating that more efficient photon capturing can be achieved when pitch $d = \lambda$ and 2λ, particularly the former. This effect can be simply explained by efficient capturing of the highest order diffraction for 700 nm wavelength. As speculated before, when d is approaching λ and 2λ, the highest order diffracted EM wave is propagating in plane inside the NWL array structures that can significantly improve photon coupling efficiency into NWLs. Particularly, 700 nm pitch yields only two diffraction orders, m = 0, 1, whereas 1.4 μm pitch yields three orders m = 0, 1, 2; thus a 700 nm pitch NWL array demonstrates better overall photon capturing efficiency than a 1.4 μm pitch NWL array. Meanwhile, Figure 3c4 also demonstrates periodic patterns inside the NWL that are not observed in Figure 3c2; this can be

dx.doi.org/10.1021/nl3014567 | Nano Lett. 2012, 12, 3682−3689

ascribed to internal scattering and interference inside the larger diameter (1.3 μm) NWL.

Leveraging advantages of periodic nanophotonic structures over random nanostructures for photon harvesting is of great importance for rational design of high performance photonic and optoelectronic devices. Recent works have shown that periodic nanophotonic structures can outperform random nanostructures in terms of photon harvesting.[22,32] Figure 2c,d has clearly shown that periodicity could lead to improved photon capturing if the pitch matches with input wavelength, which is highly consistent with the 2D absorption contour shown in Figure 3b. As the comparison, the same simulations were also performed on single NWLs with the same diameters but without applying periodic boundary condition, as shown in Figure 3d1−d4. It can be seen that the efficiency of photon coupling into NWLs simply depends on their diameters, that is, the larger the NWL diameter, the easier a photon enters the NWL. This is consistent with the past studies on optical transmission through single holes with diameter comparable to wavelength.[33] In addition, a direct comparison between Figure 3 panels c2 and d2 clearly reveals that when pitch $d = \lambda$, periodic structures greatly facilitate photon coupling into a subwavelength NWL. The same effect can be also observed when comparing Figure 3 panels c4 and d4 where $d = 2\lambda$.

It is worth noting that the existence of the absorption bands in Figure 3b instead of absorption "hot spots" corresponding to pitch-wavelength matching conditions suggests that high absorption can be achieved even there is an acceptable deviation from the matching conditions, which gives a favorable structural design window for optimal photon harvesting. On the other hand, it will naturally lead to the conjecture that for an optimized photon-harvesting structure, high optical absorption can be achieved for a broadband wavelength with a center wavelength corresponding to the pitch-wavelength matching condition. In fact, this can be easily confirmed by the strong broadband absorption for the largest NWL diameter in Figure 2a centering around 500 nm. This characteristic is particularly important for efficient photon harvesting for a broadband spectrum, such as the solar irradiance spectrum. On the other hand, the fact that Figure 3b shows two absorption bands whereas Figure 2c,d shows one absorption band indicates that NWLs with 2 μm depth and 1.4 μm pitch are less efficient for capturing 700 nm wavelength photon, as compared with those with semi-infinitive depth and the same pitch. To further confirm this observation, simulated 2D absorption contour for the 2 μm depth NWL arrays without top surface roughness was obtained and shown in Figure 4a. In this case, 700 nm input wavelength was used as well, and a single absorption band centering around 700 nm pitch along the upper boundary of the 2D contour can be clearly resolved. This fact suggests that the bottom reflection of the NWLs plays an important role in determining their photon-harvesting capability. To shed more light on this, EM wave propagation in the NWLs with 2 μm depth was simulated and shown in Figure 4b−e for NWL arrays with pitches of 400 nm, 700 nm, 1 μm, and 1.4 μm, respectively. Note that the pitches and diameters of NWLs here are identical with those shown in Figure 3c in order to make a relevant comparison among them. It can be seen that when pitch is 400 nm, which is much smaller than wavelength, the results shown in Figure 4b and 3c1 are almost the same, namely, the majority part of EM wave energy is reflected back regardless of the depth of NWLs. However, interaction between EM wave and NWLs for the rest of the three cases

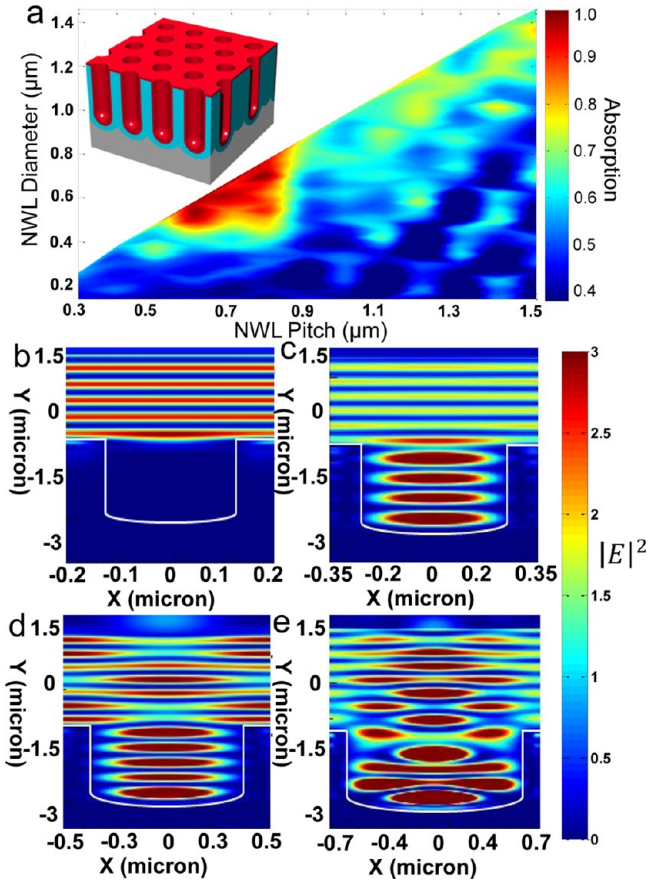

Figure 4. (a) Simulated absorption 2D contour with a monochromatic input light λ = 700 nm showing one absorption bands centering around pitch $d = \lambda$. Inset: schematic drawing of ordered NWLs with 2 μm depth and flat top surface. (b−e) $|E|^2$ cross-sectional distribution inside NWLs with pitches of 400 nm, 700 nm, 1 μm, and 1.4 μm, respectively, showing the effect of reflected EM wave from the bottom of NWLs.

shows distinctive differences. Particularly, it is clear that only 700 nm pitch condition, shown in Figure 4c, yields low reflectance, which agrees well with Figure 4a. In this case, EM wave propagation inside NWL results in energy reflection from the bottom of NWLs that slightly increases total reflectance as compared with the case shown in Figure 3c2. Meanwhile, EM wave reflection from the bottom of NWLs is much more pronounced for 1 μm (Figure 4d) and 1.4 μm (Figure 4e) pitch NWL arrays, thus the total reflectance for both cases is quite high, resulting in low absorption consistent with Figure 4a. The EM wave propagation processes for the above four cases are shown in the Supporting Information video clips. It is worth noting that 700 nm pitch NWLs show strong capturing capability for 700 nm wavelength photon, even though the NWL depth is only 2 μm. Consequently, the highest absorption reaches 97.2%, shown in Figure 4a, which is only 1.5% lower than the case in which NWLs are semi-infinitively deep, shown in Figure 3b.

Investigations on NWL arrays with both infinitive and finite depth have revealed the origin of the absorption band in the 2D absorption contours matching the wavelength of the incident photons. Nevertheless, the absorption band shown in Figure 4a is better defined with a clear boundary, as compared with the bands in Figure 2c,d, which are much more extended. This difference is attributed to the additional scattering caused by

dx.doi.org/10.1021/nl3014567 | Nano Lett. 2012, 12, 3682−3689

the periodic roughness on the top of NWL arrays in reality. To confirm this, simulated 2D absorption contour of NWL arrays with top surface roughness (inset of Figure 5, constructed

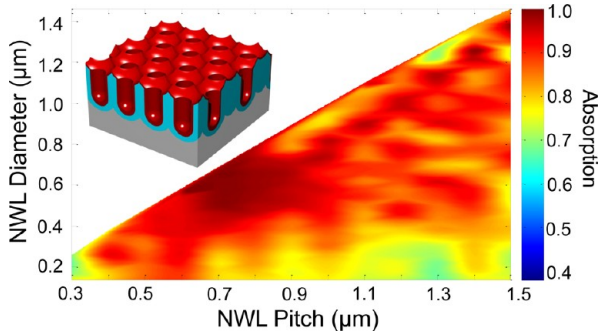

Figure 5. Simulated absorption 2D contour with a monochromatic input light λ = 700 nm showing one absorption band centering around pitch $d = \lambda$. In this case, NWLs have the actual structure fabricated in experiment. Inset: schematic drawing of the NWL structure used in simulation.

according to Supporting Information Figure S8) for 700 nm wavelengths is shown in Figure 5 in order to compare with Figure 4a directly. It is evident that the location of the hot absorption bands still matches 700 nm wavelength. However, in contrast to Figure 4a the region with over 80% absorption extends to almost the entire 2D contour, which clearly shows the effect of top surface roughness. Meanwhile, Supporting Information Figure S9 shows the results for λ = 400, 500, and 600 nm demonstrating the similar effect. These results combined together contribute to the extended absorption bands shown in Figure 2c,d.

As one unique type of nanophotonic structure, photon capturing capability of 3D NWL arrays has not yet been systematically explored previously. In this work, we have demonstrated not only a facile and scalable approach to fabricate self-organized NWL arrays with precisely controlled geometry but also presented systematic investigations of optical properties of the engineered NWL arrays with both experiments and simulations. It was discovered that a properly designed 3D NWL array can serve as an efficient photon harvester. There also exists a matching principle between the periodicity of the NWL arrays and the wavelength for the optimal photon harvesting. These findings cannot only greatly substantiate the understanding of the interplay between photons and NWLs but also serve as solid stepping stones toward implementation of novel-structured optoelectronic devices, such as solar cells and photodetectors.

■ ASSOCIATED CONTENT

Ⓢ Supporting Information

Experimental details and FDTD simulation details. This material is available free of charge via the Internet at http://pubs.acs.org.

■ AUTHOR INFORMATION

Corresponding Author

*E-mail: eezfan@ust.hk.

Author Contributions

§These authors contributed equally to this paper.

Notes

The authors declare no competing financial interest.

■ ACKNOWLEDGMENTS

This work was partially supported by DAG09/10.EG09, HKUST Research Project Competition Grant (RPC11EG38), General Research Fund (612111) from Hong Kong Research Grant Council, and National Research Foundation of Korea funded by the Korean Government (NRF-2010-220-D00060, 2008-0662256).

■ REFERENCES

(1) Zhu, J.; Yu, Z. F.; Burkhard, G. F.; Hsu, C. M.; Connor, S. T.; Xu, Y. Q.; Wang, Q.; McGehee, M.; Fan, S. H.; Cui, Y. *Nano Lett.* **2009**, *9*, 279−282.

(2) Liu, C.; Chen, C.; Chen, S.; Yen, Y.; Kuo, W.; Liao, Y.; Juang, J.; Kuo, H.; Lai, C.; Chen, L.; Chueh, Y. *Nano Lett.* **2011**, *11*, 4443−4448.

(3) Chueh, Y. L.; Fan, Z. Y.; Takei, K.; Ko, H.; Kapdia, R.; Rathore, A.; Miller, N.; Yu, K.; Wu, M.; Haller, E. E.; Javey, A. *Nano Lett.* **2010**, *10*, 520−523.

(4) Yu, R.; Ching, K.; Lin, Q.; Leung, S.; Arcrossito, D.; Fan, Z. *ACS Nano* **2011**, *5*, 9291−9298.

(5) Han, S. E.; Chen, G. *Nano Lett.* **2010**, *10*, 4692−4696.

(6) Chen, H.; Chuang, S.; Lin, C.; Lin, Y. *Opt. Express* **2007**, *15*, 14793−14803.

(7) Garnett, E. C.; Yang, P. D. *Nano Lett.* **2010**, *10*, 1082−1087.

(8) Chang, H.; Lai, K.; Dai, Y.; Wang, H.; Lin, C.; He, J. *Energy Environ. Sci.* **2011**, *4*, 2863−2869.

(9) Kelzenberg, M. D.; Boettcher, S. W.; Petykiewicz, J. A.; Turner-Evans, D. B.; Putnam, M. C.; Warren, E. L.; Spurgeon, J. M.; Briggs, R. M.; Lewis, N. S.; Atwater, H. A. *Nat. Mater.* **2010**, *9*, 239−244.

(10) Shin, J. C.; Kim, K. H.; Yu, K. J.; Hu, H.; Yin, L.; Ning, C.; Rogers, J. A.; Zuo, J.; Li, X. *Nano Lett.* **2011**, *11*, 4831−4838.

(11) Weintraub, B.; Wei, Y.; Wang, Z. L. *Angew. Chem., Int. Ed.* **2009**, *48*, 8981−8985.

(12) Fan, Z. Y.; Kapadia, R.; Leu, P. W.; Zhang, X. B.; Chueh, Y. L.; Takei, K.; Yu, K.; Jamshidi, A.; Rathore, A. A.; Ruebusch, D. J.; Wu, M.; Javey, A. *Nano Lett.* **2010**, *10*, 3823−3827.

(13) Fan, Z. Y.; Razavi, H.; Do, J. W.; Moriwaki, A.; Ergen, O.; Chueh, Y. L.; Leu, P. W.; Ho, J. C.; Takahashi, T.; Reichertz, L. A.; Neale, S.; Yu, K.; Wu, M.; Ager, J. W.; Javey, A. *Nat. Mater.* **2009**, *8*, 648−653.

(14) Wang, K. X.; Yu, Z.; Liu, V.; Cui, Y.; Fan, S. *Nano Lett.* **2012**, *12*, 1616−1619.

(15) Hsu, C.-M.; Battaglia, C.; Pahud, C.; Ruan, Z.; Haug, F.-J.; Fan, S.; Ballif, C.; Cui, Y. *Adv. Energy Mater.* **2012**, DOI: 10.1002/aenm.201100514.

(16) Yao, Y.; Yao, J.; Narasimhan, V. K.; Ruan, Z.; Xie, C.; Fan, S. H.; Cui, Y. *Nat. Commun.* **2012**, *3*, 664.

(17) Grandidier, J.; Callahan, D. M.; Munday, J. N.; Atwater, H. A. *Adv. Mater.* **2011**, *23*, 1272−1276.

(18) Peng, K.; Wang, X.; Li, L.; Wu, X.; Lee, S. *J. Am. Chem. Soc.* **2010**, *132*, 6872−6873.

(19) Han, S. E.; Chen, G. *Nano Lett.* **2010**, *10*, 1012−1015.

(20) Hernandez-Pagan, E. A.; Wang, W.; Mallouk, T. E. *ACS Nano* **2011**, *5*, 3237−3241.

(21) Qiu, J.; Guo, M.; Wang, X. *ACS Appl. Mater. Interfaces* **2011**, *3*, 2358−2367.

(22) Battaglia, C.; Hsu, C. -H.; Söderström, K.; Escarré, J.; Haug, F. -J.; Charrière, M.; Boccard, M.; Despeisse, M.; Alexander, D. T. L.; Cantoni, M.; Cui, Y.; Ballif, C. *ACS Nano* **2012**, *6* (3), 2790−2797.

(23) Zhu, J.; Hsu, C.; Yu, Z.; Fan, S.; Cui, Y. *Nano Lett.* **2010**, *10*, 1979−1984.

(24) Paudel, T.; Rybczynski, J.; Gao, Y. T.; Lan, Y. C.; Peng, Y.; Kempa, K.; Naughton, M. J.; Ren, Z. F. *Phys. Status Solidi A* **2011**, *208*, 924−927.

(25) Jessensky, O.; Muller, F.; Gosele, U. *Appl. Phys. Lett.* **1998**, *72*, 1173−1175.

(26) Steinhart, M.; Wendorff, J. H.; Greiner, A.; Wehrspohn, R. B.; Nielsch, K.; Schilling, J.; Choi, J.; Gosele, U. *Science* **2002**, *296*, 1997−1997.

(27) Fan, Z. Y.; Dutta, D.; Chien, C. J.; Chen, H. Y.; Brown, E. C.; Chang, P. C.; Lu, J. G. *Appl. Phys. Lett.* **2006**, *89*, 213110.
(28) Ergen, O.; Ruebusch, D. J.; Fang, H.; Rathore, A. A.; Kapadia, R.; Fan, Z.; Takei, K.; Jamshidi, A.; Wu, M.; Javey, A. *J. Am. Chem. Soc.* **2010**, *132*, 13972−13974.
(29) Masuda, H.; Yada, K.; Osaka, A. *Jpn. J. Appl. Phys.* **1998**, *37*, L1340−L1342.
(30) Choi, J.; Luo, Y.; Wehrspohn, R. B.; Hillebrand, R.; Schilling, J.; Gosele, U. *J. Appl. Phys.* **2003**, *94*, 4757−4762.
(31) Hutley, M. C. In *Diffraction Gratings (Techniques of Physics)*; March, N. H., Daglish, H. N., Eds.; Academic Press: London, 1982.
(32) Yu, Z.; Raman, A.; Fan, S. *Proc. Natl. Acad. Sci. U.S.A.* **2010**, *107*, 17491−17496.
(33) Genet, C.; Ebbesen, T. W. *Nature* **2007**, *445*, 39−46.